PHYSICAL REVIEW APPLIED 6, 061001 (2016)

Magnetically Tunable Invisibility of a Homogeneous Dielectric Rod with No Cover or Active Source

Yanyan Zhang, Xiyuan Cao, Yang Tang, Zhiyuan Che, Fouodji T. Yannick, and Junjie Du*

Quantum Institute for Light and Atoms, Department of Physics, School of Physics and Materials Science, East China Normal University, Shanghai 200062, China

(Received 31 July 2016; revised manuscript received 27 October 2016; published 16 December 2016)

We demonstrate the invisibility of a homogeneous ferrite rod and photonic crystals composed of such rods when an appropriate external static magnetic field (ESMF) is applied. As a naturally occurring effect, no external tool, including metamaterial and plasmonic covers or active sources, is used to hide the rod. In the invisible state, the response of the rod to the impinging wave becomes unique, with a 1/4-cycle response delay of the induced magnetic dipole which lowers its scattering efficiency to the maximum possible extent. The visible and invisible states can be manipulated by an ESMF. The manipulability enables photonic crystals composed of such rods to assume different functions in the same electromagnetic device, such as remaining transparent for the impinging wave or totally reflecting it. The fast switching time of magnetic systems might make it particularly useful for practical applications.

DOI: 10.1103/PhysRevApplied.6.061001

The hypothesis of electromagnetic (EM) invisibility, with various alternative approaches proposed and important technologies advanced in micro- and nanomaterials over the past decades, no longer belongs to the realm of science fiction. Metamaterials pave the way to realizing the invisibility by designing a cloak based on a conformal transformation of coordinates [1–10], anomalous localized resonances [11,12], or the construction of complementary media [13]. Plasmonic shells can also function as a cloak by producing a scattering cancellation with the cloaked object [14–18]. Along with metamaterial and plasmonic covers, active sources are a tool for concealing an object by elaborately tailoring their magnitudes and phases [19–21]. These invisibility techniques, with no exception, rely on the utilization of external tools.

The invisibility technique, based on intrinsic mechanisms rather than external tools, has the potential to develop EM devices with unique advantages. The intrinsic mechanism of EM scattering can be understood from the viewpoint of the response of induced multipoles inside particles to the impinging field since EM scattering originates from the reradiation of these multipoles. Therefore, an approach to making a particle with a particular geometry hide itself is to excite the desired multipoles inside it so that they interfere destructively to suppress the scattering [22]. The alignment of the dark-state frequencies, which are explained as a consequence of the destructive interference between multipoles, can result in the invisibility of a corrugated rod [23]. The Fano resonance state originating from the interaction between a narrow resonant band and a broad background can produce multipole-destructive interference and make a homogeneous high-permittivity dielectric particle self-invisible [24]. Here, we demonstrate that the unique response of induced multipoles to impinging waves might be another intrinsic mechanism for making a particle conceal itself.

It has been shown that the EM response of an isolated ferrite rod can be very special, with a circular dipole excited due to its nonsymmetric angular momenta components of opposite signs $\pm n$ in Mie-scattering theory [25–28]. This particular property has been used to achieve unidirectional EM edge states [29–34] in ferrite photonic crystals. Here, we study a ferrite rod whose scattering is dominated by the monopolar and dipolar reradiation which correspond, respectively, to the contributions of the angular-momenta components 0 and ± 1 in a Mie expansion. The response of the induced multipoles is unique. The dipole has a 1/4-cycle response delay to the impinging field, which makes itself extremely weak. These multipoles nearly fail to produce reradiation, and the homogeneous rod becomes invisible even though no cover or active source is used. Because of the dependence of the permeability and, furthermore, its scattering property on the external static magnetic field (ESMF), the invisible and visible states of ferrite rods can be manipulated by the ESMF. Compared to the water-temperature tunability in the invisibility of a high-permittivity dielectric rod [24], the magnetic manipulation can have a higher modulation efficiency due to the fast switching time of magnetic systems, and the technique can be more easily realized in practical applications.

The invisibility of homogeneous rods might expand the application versatility of artificially structured EM materials. Here, we study a photonic crystal (PC) composed of such rods and show that it is also invisible for the impinging wave with an arbitrary angle of incidence, meaning that the

*phyjunjie@gmail.com

EM wave passes through it without being perturbed. However, it may prevent the EM wave from penetrating itself and may produce the total-reflection effect when the ESMF is changed. The ferrite PC in the invisible state operates in a special photonic passband which has not yet been studied, though the formation mechanisms [35] and the magnetic tunability [35–37] of its photonic stop band have been explored. We show that such a PC might assume different functions in an optical unit with different ESMFs applied.

The ferrite rods we study have the radius r_s and the rod axis is along the z direction. When fully magnetized, the ferrite has the magnetic permeability tensor [35,36,38]

$$\hat{\mu} = \begin{pmatrix} \mu_r & -i\mu_\kappa & 0 \\ i\mu_\kappa & \mu_r & 0 \\ 0 & 0 & 1 \end{pmatrix},$$
$$\mu_r = 1 + \frac{\omega_m(\omega_0 - i\alpha\omega)}{(\omega_0 - i\alpha\omega)^2 - \omega^2},$$
$$\mu_\kappa = \frac{\omega_m\omega}{(\omega_0 - i\alpha\omega)^2 - \omega^2}, \quad (1)$$

where α is a damping coefficient which has a negligible value on the order of 10^{-4} for many ferrites. $\omega_0 = 2\pi\gamma H_0$ is the resonance circular frequency, with $\gamma = 2.8$ MHz/Oe being the gyromagnetic ratio and H_0 the sum of the ESMFs applied in the z direction and the shape anisotropy field, while $\omega_m = 2\pi\gamma M_s$ is the characteristic circular frequency, with M_s being the saturation magnetization along the z direction. In our calculation, we use $\alpha = 5 \times 10^{-4}$, $M_s = 1750$ Oe, and the permittivity $\varepsilon_s = 25$, typical for single-crystal yttrium-iron-garnet (YIG) ferrite [38].

We plot in Fig. 1 the electric- (E-) field distribution around a rod made up of such materials, with $r_s = 3$ mm, when a transverse-magnetic plane wave with its electric field polarized along the rod axis is impinging on it. The impinging wavelength is $\lambda = 116.8$ mm. One can see that the rod is effectively "invisible" when the ESMF $H_0 = 460$ Oe in Fig. 1(a), while it becomes "visible" when $H_0 = 476$ Oe in Fig. 1(b) for the same impinging wave. The rod in the invisible state seems so small that it vanishes into its surroundings, but it seems so large that the impinging wave

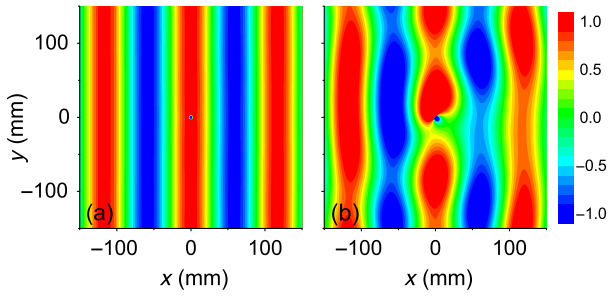

FIG. 1. The E-field distribution around the rod when (a) the ESMF $H_0 = 460$ Oe and (b) the ESMF $H_0 = 476$ Oe.

is significantly perturbed when the ESMF is changed. Obviously, the response mechanism inside the rod will change with the switching between invisibility and visibility when the ESMF varies since no metamaterial or plasmonic covers exist outside the rod.

Now let us see what happens inside the invisible rod based on the Mie-scattering theory. In the Mie expansion, the impinging and scattered electric fields can be written as $E_i = e^{i(\mathbf{k}\cdot\mathbf{r}-\phi_0)} = \sum_n i^n q_n J_n(x) e^{in\phi}$ and $E_s = \sum_n i^n b_n H_n^{(1)}(x) e^{in\phi}$. Here, ϕ_0 is the phase shift of the impinging field, ϕ is the polar coordinate, $x = 2\pi r/\lambda$, and the n in summation $\sum_n$ runs from $-\infty$ to $+\infty$, with the nth term denoting the nth angular-momentum channel [39]. J_n and $H_n^{(1)}$ are the nth-order Bessel function and the Hankel function of the first kind, respectively. The scattering-field coefficient b_n is connected with the impinging one q_n by the Mie-scattering coefficient α_n; i.e., $b_n = \alpha_n q_n$. The α_n with $n = 0, +1, -1$, respectively, is plotted as a function of the ESMF in Fig. 2(a) since those three components contribute the most to the scattering. One can see that they simultaneously tend to vanish when the invisibility occurs in the vicinity of $H_0 = 411$ Oe and $H_0 = 460$ Oe. Therefore, these important scattering-field coefficients b_n are very small in the invisible state. On the other hand, the scattering of the rod keeps changing during one wave cycle. This flux can be seen from the fact that q_n depends on the phase shift of the impinging wave ϕ_0 (when the phase shift ϕ_0 changes from 0 to 2π, equivalently, the wave travels in one period T). Without loss of generality, the impinging field is assumed to propagate along the x direction, so $q_n = e^{-i\phi_0}$. Intuitively, one expects that the stronger scattering will occur when a crest (trough) $\phi_0 = 0$ ($\phi_0 = \pi$) arrives at the rod center. However, our data show that the scattering field remains negligibly small for any ϕ_0 and even achieves the smallest value in the crest (trough) position. This approach draws our attention to the response of the rod over one wave cycle in order to understand what leads to the vanishing α_n.

The response of a rod depends on how the induced multipoles inside it respond to the impinging wave [40]. The induced monopole corresponds to the component $n = 0$, with the isotropic inner and outer scattered fields [25]. While the components $n = -1$ and $n = +1$ denote a clockwise and a counterclockwise rotating magnetic-dipole moment, respectively, and their superposition will result, in general, in a linear oscillating magnetic dipole along the propagation direction [25,26]. When $\phi_0 = 0$—i.e., when the crest arrives at the rod center [shown by the solid red line in Fig. 2(b)]—Figs. 2(c) and 2(d) demonstrate that the two excited, rotating magnetic-dipole moments inside the invisible rod have the opposite direction and will, obviously, cancel each other out. This result shows that the rod has the weakest response to the strongest field during one wave cycle. When $\phi_0 = \pi/2$ (the magnitude of the impinging field is zero at the rod center), as displayed by

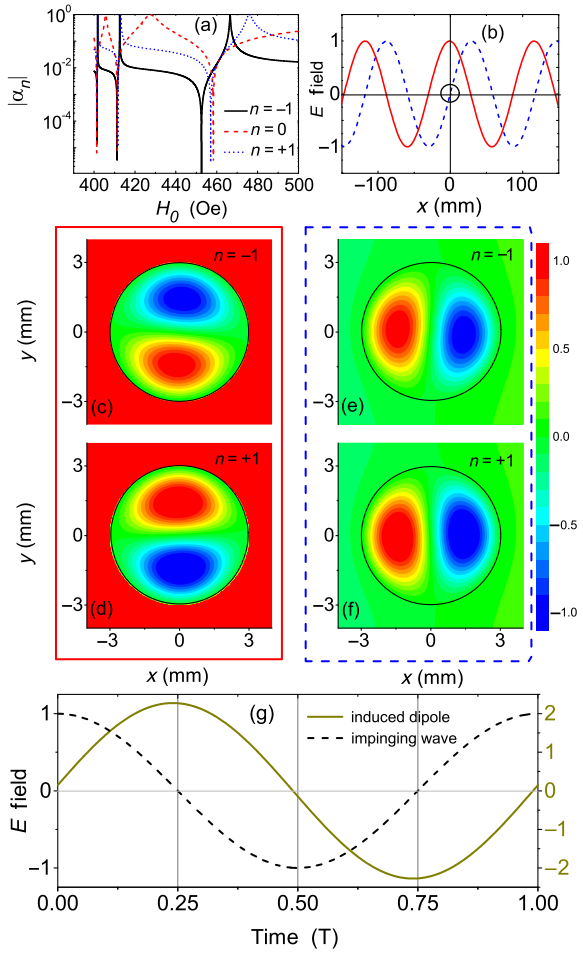

FIG. 2. (a) The absolute value of Mie-scattering coefficients $|\alpha_{-1}|$, $|\alpha_0|$, and $|\alpha_{+1}|$ versus the ESMF when the wavelength $\lambda = 116.8$ mm. (b) The impinging field when ϕ_0 changes from 0 to $\pi/2$. The inner field in the components (c) [(e)] $n = -1$ and (d) [(f)] $n = +1$ when the rod center is located at the crest (the zero-magnitude position) of the impinging wave. The black circle denotes the rod and the total field is plotted outside the rod. (g) The time dependence of the impinging field and the field from the induced dipole. The dipole has a 1/4-cycle response delay relative to the impinging field.

the dashed blue line in Fig. 2(b), the two rotating magnetic-dipole moments, illustrated by Figs. 2(e) and 2(f), will constructively interfere. However, because the impinging field is zero at the rod center, the linear oscillating magnetic dipole is so weak that its radiation is negligible. Overall, the components $n = \pm 1$ have a 1/4-cycle response delay to the impinging wave. The response delay is displayed in Fig. 2(g) by comparing the dipolar-radiation field and the impinging wave $E_i = e^{i(\mathbf{k}\cdot\mathbf{r}-\omega t)}$ in one period T. The delay makes it impossible to produce the large Mie-scattering coefficient $\alpha_{\pm 1}$. It should be emphasized that the response delay of the angular-momenta components is usually much smaller than 1/4 of a cycle and not very obvious. The 1/4-cycle delay lowers the dipolar-radiation efficiency to the maximum possible extent, and therefore the induced magnetic dipole makes no contribution to the scattering. The advantage of the response delay is that the suppression of the scattering does not rely on the introduction of the corrugation into the rod [23], enhancing the possibility of applications. At the same time, the scattering from the component $n = 0$ is also negligible for two reasons when the invisibility occurs. First, the Mie-scattering coefficient α_0 becomes very small, as illustrated in Fig. 2(a). This result shows that it is a very weak monopole. Second, its isotropic nature results in the weak scattered energy's being equally distributed in all directions and decaying to zero quickly. Since the components $n = 0$ and $n = \pm 1$ make a negligible contribution to the scattering, the homogeneous rod with no cover will be invisible to an external observer, as shown in Fig. 1(a).

These weak induced multipoles can only make an effect on the very-near field of the rod. Thus, we will evaluate the invisibility performance by examining the scattered field and its decay from the rod surface. Since the induced linear oscillating magnetic dipole is oriented perpendicular to the impinging wave, the near field is strongest in the impinging direction. Figure 3(a) displays the scattered electric field along a line in the impinging direction (the x direction). One can see that the maximum value $E = 0.1$ of the scattered field appears at the surface of the rod and exponentially decays to zero. Compared to the impinging wave with the maximum value $E = 1$, the weak scattering has no effect on it and a good invisibility is achieved.

When considering practical applications, one expects multirod systems to also be invisible [17]. We first consider a single-rod-layer array which has the lattice spacing $a_0 = \lambda/5$. Since the very weak induced linear oscillating magnetic dipole is oriented perpendicular to the impinging direction, the individual rod scatters nearly no wave in the direction transverse to the impinging wave. Thus, the inter-rod interaction will be very weak, even though the rods are placed in close proximity to one another when the rod array is perpendicular to the impinging wave. Thus, Fig. 3(b) shows that the impinging field is not perturbed, and the whole array is in the invisible state. However, when the

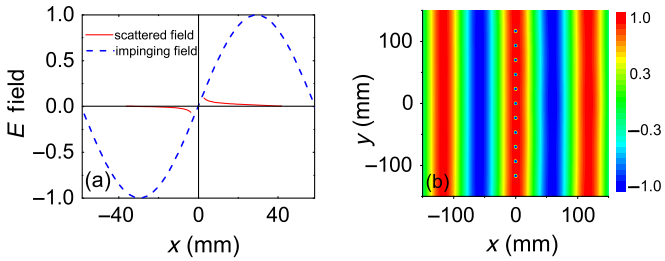

FIG. 3. (a) The comparison between the scattered (red solid line) and the impinging field (blue dashed line) outside the invisible rod along the incident direction (the x direction). (b) The E-field distribution around an array of rods in the invisible state in the normal incidence case.

impinging direction is changed, the reflection by the array will be evident. This reflection occurs because the dipolar radiation has an angular width which causes the inter-rod coupling when the dipole moments are not parallel to the array in the small-spacing case ($a_0 = \lambda/5$).

Furthermore, we expect that multiple-layer rod arrays can be also invisible since the weak scattering of an individual rod quickly decays to zero and only has an effect on the near-field region. As an example, let us consider a square-lattice PC with a larger lattice spacing, $a_0 = \lambda/2$. When $H_0 = 460$ Oe, at which point the individual rod is electromagnetically invisible, Fig. 4(a) demonstrates that the impinging wave is unperturbed by the presence of the PC. However, it is totally reflected in Fig. 4(d) when $H_0 = 476$ Oe, at which point the rod is electromagnetically visible. Therefore, such a PC can effectively tune the propagation direction of EM waves and can function as an EM switch. For a PC which has a line defect with a sharp corner, Fig. 4(b) shows that the impinging wave propagates through the PC without being perturbed when $H_0 = 460$ Oe, while the impinging wave is coupled into the line defect and then travels smoothly around the corner, as shown in Fig. 4(e). As is common knowledge, the variation of ESMFs can cause the shift of photonic band gaps of ferrite PCs [35,36]. Similarly, the comparison between Figs. 4(c) and 4(f) shows that the stop band shifts to higher frequencies when the ESMF increases, and a photonic passband in the invisibility case [Figs. 4(a) and 4(b)] becomes a complete photonic stop band in the total-reflection and waveguide case [Figs. 4(d) and 4(e)]. It should be emphasized that the invisibility state is a special photonic passband in which the EM properties of the material appear to be identical to air and the impinging wave does not have the waveform distortion or the phase delay. This fact helps us avoid the distortion of signal carried by the impinging EM wave and improve the performance of EM devices. In the usual switching effect, which depends only on the shift of the stop band and does not involve invisibility, the phase of the outgoing wave has a delay, in contrast to that of the impinging wave [37]. In addition, a PC can assume different functions when it operates in the invisibility state or a complete stop band by tuning the ESMF.

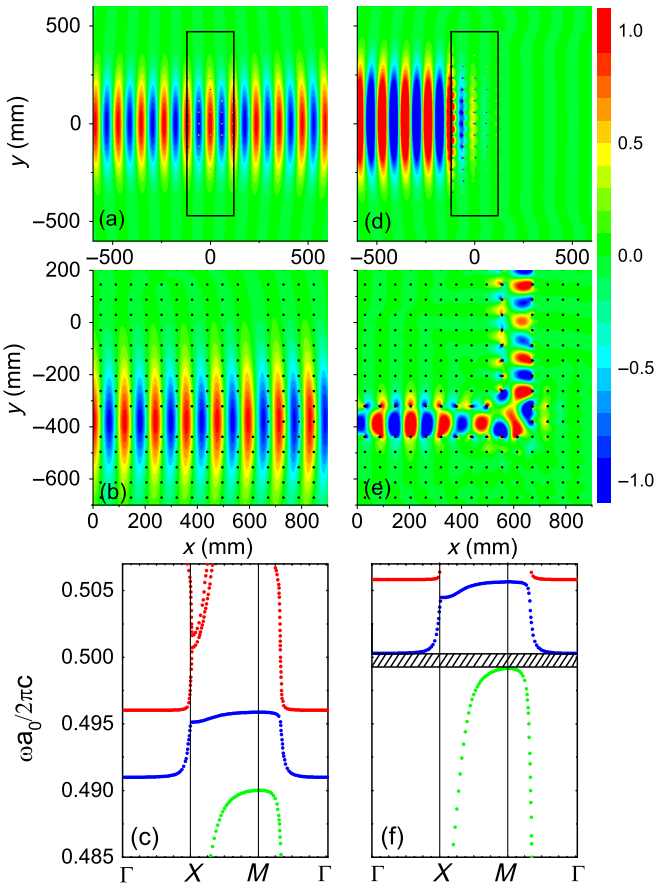

FIG. 4. The E-field distribution around a PC when (a) the ESMF $H_0 = 460$ Oe and (d) the ESMF $H_0 = 476$ Oe. The E-field distribution around a PC which has a line defect with a sharp corner when (b) the ESMF $H_0 = 460$ Oe and (e) the ESMF $H_0 = 476$ Oe. Photonic band structure of the PC when (c) the ESMF $H_0 = 460$ Oe and (f) the ESMF $H_0 = 476$ Oe.

The invisibility of the PC in Fig. 4 occurs for the impinging wave with an arbitrary angle of incidence. Figures 2(c)–2(f) show that the direction of the induced weak dipole moment is always perpendicular to the impinging wave. Thus, the strongest interaction between layers happens in the normal-incidence case for a square-lattice PC. When the scattered waves of a normal incident wave cannot arrive at the adjacent rod layer, the whole PC is also necessarily invisible for waves with any other impinging angles. Here, we choose a larger spacing a_0 in order to eliminate the coupling between layers, in contrast to the case in Fig. 3(b). $a_0 = \lambda/2$ (in Fig. 4) is a typical size, which not only makes the existence of the complete band gap possible but also guarantees the occurrence of the invisibility for the PC.

The size of the invisible object is limited when metamaterial covers are used because they rely on specific anisotropic and inhomogeneous material responses. The invisibility for collections of objects by plasmonic covers has been studied and it has been shown that an system at the scale of the wavelength can be invisible [17]. Obviously, the invisible PC in Fig. 4 may have arbitrary size since the technique originates from the invisibility of the constituting rods.

In summary, we show the EM invisibility of a homogeneous ferrite rod with no cover and an active source. The invisible state is realized when the induced magnetic dipole has a 1/4-cycle response delay under an appropriate ESMF. The visible and invisible states can be manipulated by the ESMF. PCs composed of such rods can also be invisible for EM waves with an arbitrary angle of incidence. This quality

leads to the possibility of improving the performance of EM devices.

This work was supported by NSFC (Grant No. 11474098) and the Innovation Program of the Shanghai Municipal Education Commission (Grant No. 14ZZ049).

[1] J. B. Pendry, D. Schurig, and D. R. Smith, Controlling electromagnetic fields, Science **312**, 1780 (2006).

[2] D. Schurig, J. J. Mock, B. J. Justice, S. A. Cummer, J. B. Pendry, A. F. Starr, and D. R. Smith, Metamaterial electromagnetic cloak at microwave frequencies, Science **314**, 977 (2006).

[3] J. Li and J. B. Pendry, Hiding under the Carpet: A New Strategy for Cloaking, Phys. Rev. Lett. **101**, 203901 (2008).

[4] J. Valentine, J. Li, T. Zentgraf, G. Bartal, and X. Zhang, An optical cloak made of dielectrics, Nat. Mater. **8**, 568 (2009).

[5] T. Ergin, N. Stenger, P. Brenner, J. B. Pendry, and M. Wegener, Three-dimensional invisibility cloak at optical wavelengths, Science **328**, 337 (2010).

[6] W. Cai, U. K. Chettiar, A. V. Kildishev, and V. M. Shalaev, Optical cloaking with metamaterials, Nat. Photonics **1**, 224 (2007).

[7] U. Leonhardt, Optical conformal mapping, Science **312**, 1777 (2006).

[8] H. Y. Chen, Z. X. Liang, P. J. Yao, X. Y. Jiang, H. R. Ma, and C. T. Chan, Extending the bandwidth of electromagnetic cloaks, Phys. Rev. B **76**, 241104 (2007).

[9] Z. Jacob and E. E. Narimanov, Semiclassical description of non-magnetic cloaking, Opt. Express **16**, 4597 (2008).

[10] A. V. Kildishev and V. M. Shalaev, Engineering space for light via transformation optics, Opt. Lett. **33**, 43 (2008).

[11] G. W. Milton and N. A. Nicorovici, On the cloaking effects associated with anomalous localized resonance, Proc. R. Soc. A **462**, 3027 (2006).

[12] N. A. Nicorovici, G. W. Milton, R. C. McPhedran, and L. C. Botten, Quasistatic cloaking of two-dimensional polarizable discrete systems by anomalous resonance, Opt. Express **15**, 6314 (2007).

[13] Y. Lai, J. Ng, H. Y. Chen, D. Z. Han, J. J. Xiao, Z. Q. Zhang, and C. T. Chan, Illusion Optics: The Optical Transformation of an Object into Another Object, Phys. Rev. Lett. **102**, 253902 (2009).

[14] A. Alù and N. Engheta, Achieving transparency with plasmonic and metamaterial coatings, Phys. Rev. E **72**, 016623 (2005).

[15] A. Alù and N. Engheta, Plasmonic materials in transparency and cloaking problems: Mechanism, robustness, and physical insights, Opt. Express **15**, 3318 (2007).

[16] M. G. Silveirinha, A. Alù, and N. Engheta, Parallel-plate metamaterials for cloaking structures, Phys. Rev. E **75**, 036603 (2007).

[17] A. Alù and N. Engheta, Cloaking and transparency for collections of particles with metamaterial and plasmonic covers, Opt. Express **15**, 7578 (2007).

[18] A. Alù and N. Engheta, Multi-frequency Optical Invisibility Cloaks with Layered Plasmonic Shells, Phys. Rev. Lett. **100**, 113901 (2008).

[19] D. A. B. Miller, On perfect cloaking, Opt. Express **14**, 12457 (2006).

[20] F. G. Vasquez, G. W. Milton, and D. Onofrei, Active Exterior Cloaking for the 2D Laplace and Helmholtz Equations, Phys. Rev. Lett. **103**, 073901 (2009).

[21] J. J. Du, S. Y. Liu, and Z. F. Lin, Broadband optical cloak and illusion created by the low order active sources, Opt. Express **20**, 8608 (2012).

[22] A. E. Miroshnichenko, A. B. Evlyukhin, Y. F. Yu, R. M. Bakker, A. Chipouline, A. I. Kuznetsov, B. Lukyanchuk, B. N. Chichkov, and Y. S. Kivshar, Nonradiating anapole modes in dielectric nanoparticles, Nat. Commun. **6**, 8069 (2015).

[23] D. Ye, L. Lu, J. D. Joannopoulos, M. Soljačić, and L. Ran, Invisible metallic mesh, Proc. Natl. Acad. Sci. U.S.A. **113**, 2568 (2016).

[24] M. V. Rybin, D. S. Filonov, P. A. Belov, Y. S. Kivshar, and M. F. Limonov, Switching from visibility to invisibility via Fano resonances: Theory and experiment, Sci. Rep. **5**, 8774 (2015).

[25] J. J. Du, Z. F. Lin, S. T. Chui, G. J. Dong, and W. P. Zhang, Nearly Total Omnidirectional Reflection by a Single Layer of Nanorods, Phys. Rev. Lett. **110**, 163902 (2013).

[26] J. J. Du, Z. F. Lin, S. T. Chui, W. L. Lu, H. Li, A. Wu, Z. Sheng, J. Zi, X. Wang, S. C. Zou, and F. W. Gan, Optical Beam Steering Based on the Symmetry of Resonant Modes of Nanoparticles, Phys. Rev. Lett. **106**, 203903 (2011).

[27] F. J. Rodríguez-Fortuño, G. Marino, P. Ginzburg, D. O'Connor, A. Martínez, G. A. Wurtz, and A. V. Zayats, Near-field interference for the unidirectional excitation of electromagnetic guided modes, Science **340**, 328 (2013).

[28] T. J. Guo, T. F. Li, M. Yang, H. X. Cui, Q. H. Guo, X. W. Cao, and J. Chen, Nonreciprocal optical diffraction by a single layer of gyromagnetic cylinders, Opt. Express **22**, 537 (2014).

[29] F. D. M. Haldane and S. Raghu, Possible Realization of Directional Optical Waveguides in Photonic Crystals with Broken Time-Reversal Symmetry, Phys. Rev. Lett. **100**, 013904 (2008).

[30] Z. Wang, Y. D. Chong, J. D. Joannopoulos, and M. Soljčić, Reflection-Free One-Way Edge Modes in a Gyromagnetic Photonic Crystal, Phys. Rev. Lett. **100**, 013905 (2008).

[31] Z. Wang, Y. D. Chong, J. D. Joannopoulos, and M. Soljačić, Observation of unidirectional backscattering-immune topological electromagnetic states, Nature (London) **461**, 772 (2009).

[32] Y. Poo, R. X. Wu, Z. F. Lin, Y. Yang, and C. T. Chan, Experimental Realization of Self-Guiding Unidirectional Electromagnetic Edge States, Phys. Rev. Lett. **106**, 093903 (2011).

[33] S. Y. Liu, W. L. Lu, Z. F. Lin, and S. T. Chui, Molding reflection from metamaterials based on magnetic surface plasmons, Phys. Rev. B **84**, 045425 (2011).

[34] Y. Poo, R. X. Wu, S. Y. Liu, Y. Yang, Z. F. Lin, and S. T. Chui, Experimental demonstration of surface morphology independent electromagnetic chiral edge states originated from magnetic plasmon resonance, Appl. Phys. Lett. **101**, 081912 (2012).

[35] S. Y. Liu, J. J. Du, Z. F. Lin, R. X. Wu, and S. T. Chui, Formation of robust and completely tunable resonant photonic band gaps, Phys. Rev. B **78**, 155101 (2008).

[36] S. Y. Liu, W. K. Chen, J. J. Du, Z. F. Lin, S. T. Chui, and C. T. Chan, Manipulating Negative-Refractive Behavior with a Magnetic Field, Phys. Rev. Lett. **101**, 157407 (2008).

[37] H. J. Chen and S. Y. Liu, Manipulating electromagnetic wave with the magnetic surface plasmon based metamaterials, Appl. Phys. A **107**, 363 (2012).

[38] D. M. Pozar, *Microwave Engineering*, 3rd ed. (John Wiley & Sons, New York, 2004).

[39] H. C. Van De Hulst, *Light Scattering by Small Particles* (Dover Publications, New York, 1981).

[40] R. Paniagua-Domínguez, Y. F. Yu, A. E. Miroshnichenko, L. A. Krivitsky, Y. H. Fu, V. Valuckas, L. Gonzaga, Y. T. Toh, A. Y. S. Kay, B. Lukyanchuk, and A. I. Kuznetsov, Generalized Brewster effect in dielectric metasurfaces, Nat. Commun. **7**, 10362 (2016).